Multiwfn: A Multifunctional Wavefunction Analyzer

Tian Lu[a]* and Feiwu Chen[a]

Multiwfn is a multifunctional program for wavefunction analysis. Its main functions are: (1) Calculating and visualizing real space function, such as electrostatic potential and electron localization function at point, in a line, in a plane or in a spatial scope. (2) Population analysis. (3) Bond order analysis. (4) Orbital composition analysis. (5) Plot density-of-states and spectrum. (6) Topology analysis for electron density. Some other useful utilities involved in quantum chemistry studies are also provided. The built-in graph module enables the results of wavefunction analysis to be plotted directly or exported to high-quality graphic file. The program interface is very user-friendly and suitable for both research and teaching purpose. The code of Multiwfn is substantially optimized and parallelized. Its efficiency is demonstrated to be significantly higher than related programs with the same functions. Five practical examples involving a wide variety of systems and analysis methods are given to illustrate the usefulness of Multiwfn. The program is free of charge and open-source. Its precompiled file and source codes are available from http://multiwfn.codeplex.com. © 2011 Wiley Periodicals, Inc.

DOI: 10.1002/jcc.22885

Introduction

According to quantum theory, a system wavefunction contains all information needed. However, it is often a rather complicated function and may be viewed as a black box. In common quantum chemistry calculations only energy is usually extracted. Evidently, this is insufficient to fully interpret intrinsic characteristics of electron structures. To obtain more information of chemical interest, wavefunction analysis technologies[1,2] must be used for further disclosing the black box. Unfortunately, only minimal wavefunction analysis methods are available in most of mainstream quantum chemistry packages. Although there are plenty of standalone wavefunction analysis programs,[3–8] some are limited to certain analysis techniques and some are inconvenient to use or have low efficiency. We feel that it is quite meaningful to develop a new program that integrated most of important wavefunction analysis methods, meanwhile, and is very easy to use and have high efficiency.

Multiwfn is such a wavefunction analyzer running on Windows and Linux platform. It is especially good at visual study of real space functions such as electrostatic potential (ESP) and electron localization function (ELF).[9] Multiwfn accepts wavefunctions in PROAIM format, which has been supported by many quantum chemistry packages. Some other file types such as Gaussian formatted checkpoint file and NBO plot files are also supported. Multiwfn is free and open source. Its size is very small (about 3MB). The latest version can be downloaded at http://multiwfn.codeplex.com.

The rest of this article is organized as follows: Section "Theoretical Backgrounds" briefs involved theoretical backgrounds, Section "Program" introduces various aspects of Multiwfn, in Section "Efficiency," efficiency comparison between Multiwfn and related programs is given, and Section "Practical Applications" presents five practical applications to illustrate the usefulness of Multiwfn.

Theoretical Backgrounds

Real space functions

Visualization of real space functions is an important and convenient way of studying electron structure. Multiwfn supports almost all valuable real space functions, and they will be sketched in turn. The functions involved from Sections "electron density" to "sign(λ_2)*ρ" are purely based on electron density and, thus, they can be obtained not only by quantum chemistry calculations but also by experimental techniques such as X-ray diffraction. The functions involved from Sections "value of orbital wavefunction" to "Fermi hole and Fermi correlation factor function" are directly based on wavefunctions, and they are useful but unobservable experimentally. Three special real space functions presented in Multiwfn are briefed in Sections "ESP from nuclear or atomic charges" and "promolecular and deformation properties."

Electron density

$$\rho(\mathbf{r}) = \sum_i \eta_i |\varphi_i(\mathbf{r})|^2 = \sum_i \eta_i \left| \sum_l C_{l,i} \chi_l(\mathbf{r}) \right|^2, \quad (1)$$

where φ and η correspond to the natural orbital and its occupation number, respectively. χ denotes basis function, and C is coefficient matrix.

[a] T. Lu, F. Chen
Department of chemistry and chemical engineer, School of Chemical and Biological Engineering, University of Science and Technology Beijing, Beijing 100083, People's Republic of China
E-mail: sobereva@sina.com

Contract/grant sponsor: National Natural Science foundation of China; contract/grant number: 20773011.

Gradient norm of electron density

$$|\nabla\rho(\mathbf{r})| = \sqrt{\left(\frac{\partial\rho(\mathbf{r})}{\partial x}\right)^2 + \left(\frac{\partial\rho(\mathbf{r})}{\partial y}\right)^2 + \left(\frac{\partial\rho(\mathbf{r})}{\partial z}\right)^2}. \quad (2)$$

Laplacian of electron density

$$\nabla^2\rho(\mathbf{r}) = \frac{\partial^2\rho(\mathbf{r})}{\partial x^2} + \frac{\partial^2\rho(\mathbf{r})}{\partial y^2} + \frac{\partial^2\rho(\mathbf{r})}{\partial z^2}. \quad (3)$$

The positive and negative values correspond to electron density locally depleted and concentrated, respectively. The relationships between $\nabla^2\ \rho$ and valence shell electron pair repulsion model, chemical bond type, electron localization, and chemical reactivity have been built.[10–12]

Electron spin density and spin polarization parameter Spin density is defined as follows:

$$\rho^s(\mathbf{r}) = \rho^\alpha(\mathbf{r}) - \rho^\beta(\mathbf{r}). \quad (4)$$

A similar function named spin polarization parameter[13] is expressed as follows:

$$\zeta(\mathbf{r}) = \frac{\rho^\alpha(\mathbf{r}) - \rho^\beta(\mathbf{r})}{\rho^\alpha(\mathbf{r}) + \rho^\beta(\mathbf{r})}. \quad (5)$$

The absolute value of ζ going from zero to unity corresponds to local region going from unpolarized case to completely polarized case.

Electrostatic potential

$$V_{tot}(\mathbf{r}) = V_{nu}(\mathbf{r}) + V_{ele}(\mathbf{r}) = \sum_A \frac{Z_A}{|\mathbf{r} - \mathbf{R}_A|} - \int \frac{\rho(\mathbf{r}')}{|\mathbf{r} - \mathbf{r}'|} d\mathbf{r}'. \quad (6)$$

2This function measures the electrostatic interaction between a unit point charge placed at **r** and the system of interest. A positive (negative) value implies that current position is dominated by nuclear (electronic) charges. Molecular ESP has been widely used for prediction of nucleophilic and electrophilic sites for a long time. It is also valuable in studying hydrogen bonds, halogen bonds, molecular recognitions, and the intermolecular interaction of aromatics.[14] Moreover, on the basis of statistical analysis, Murray et al. found a set of functions called GIPF,[15] which connects ESP in molecular surface and macroscopic properties. The links between ESP and covalent radii, electronegativity, and system energy were reviewed in Ref. [16].

Local information entropy: Information entropy[17] is a quantification of information, and this theory was proposed by Shannon in his study of information transmission in noise channel; nowadays, its application has been largely widened to other areas, including theoretical chemistry. For example, Aslangul et al. attempted to decompose diatomic and triatomic molecules into mutually exclusive space by minimizing information entropy[18]; Parr et al. discussed the relationship between information entropy and atom partition as well as molecular similarity.[19,20] The formula of Shannon's information entropy for normalized and continuous probability function is as follows:

$$S = -\int P(x)\ln P(x)dx. \quad (7)$$

For chemical system, if $P(x)$ is replaced by $\rho(\mathbf{r})/N$, then the integrand may be called local information entropy of electrons

$$s(\mathbf{r}) = -(\rho(\mathbf{r})/N)\ \ln(\rho(\mathbf{r})/N). \quad (8)$$

Reduced density gradient: Reduced density gradient (RDG)[21] is defined as (constant coefficient is ignored) follows:

$$\mathrm{RDG}(\mathbf{r}) = \frac{|\nabla\rho(\mathbf{r})|}{\rho^{4/3}(\mathbf{r})}. \quad (9)$$

The original intention for introducing RDG is to convert density gradient, namely eq. (2), to a dimensionless quantity. Recently, Johnson et al. found that the isosurface of RDG is a very valuable tool for revealing weak interaction regions.[22] The mechanism is easy to be explained by Table 1.

Table 1. The magnitude of electron density, its gradient norm, and reduced density gradient in different area.

	Around nuclei	Around chemical bond	Weak interaction region	Edge of molecule
$\|\nabla\rho(\mathbf{r})\|$	Large	0–Minor	0–Small	Very small–Small
$\rho(\mathbf{r})$	Large	Medium	Small	0–Small
RDG($\mathbf{r}$)	Medium	0–Minor	0–Medium	Medium–Very large

From Table 1, it is clear that different area can be distinguished according to different magnitude of real space functions. In the low electron density area, the RDG isosurfaces with small isovalue reveal a weak interaction region.

Sign(λ_2)*ρ: In Bader's QTAIM theory[11] (also see below), (3,−1) type critical point (CP) usually appears in chemical bond path or between atom pairs that have weak attractive interaction, whereas (3,+1) generally appears in the center of ring system and displays steric effect. The criterion for distinguishing (3,−1) and (3,+1) is the sign of λ_2, that is, the second largest eigenvalue of Hessian matrix of electron density. Besides, the strength of weak interaction has positive correlation with ρ (**r**). Hence, a new function can be defined as follows[22]:

$$\Lambda(\mathbf{r}) = \mathrm{Sign}(\lambda_2(\mathbf{r}))\rho(\mathbf{r}). \quad (10)$$

where the Sign is the operator used to extract the sign of variable. If the value of $\Lambda(\mathbf{r})$ is represented by colors and mapped onto RDG isosurfaces, then not only the region of weak interaction but also the type and strength are revealed visually. We will illustrate the power of this visual analysis method by practical examples in Section "weak interaction analysis of urea crystal."

Weak interaction has significant influence on conformation of macromolecules and binding mode of proteins and ligands; unfortunately, reproduction of electron density by *ab initio* and grid data calculation of RDG and Sign(λ_2)*ρ for such huge systems are always too time consuming. However, electron

density can be approximately constructed by superposing electron densities of free-state atoms, which are the so-called promolecular approximation. Johnson et al. found that weak interaction analysis under this approximate density is still reasonable.[22] The fitted densities of free-state atoms by Slater-type orbitals are already prebuilt in Multiwfn.

Value of orbital wavefunction:

$$\varphi_i(\mathbf{r}) = \sum_I C_{I,i}\chi_I(\mathbf{r}). \quad (11)$$

Hamiltonian kinetic energy density: The kinetic energy density is not uniquely defined,[11,23] because the expected value of kinetic energy operator $< \psi| -(1/2)\nabla^2|\psi >$ can be recovered by integrating kinetic energy density from alternative definitions. One of commonly used definition is as follows:

$$K(\mathbf{r}) = -\frac{1}{2}\sum_i \eta_i \varphi_i^*(\mathbf{r})\nabla^2\varphi_i(\mathbf{r}). \quad (12)$$

Lagrangian kinetic energy density: The shortcoming of Hamiltonian kinetic energy density is that the value is not always positive and real, another definition that has more clear physical meaning is as follows:

$$G(\mathbf{r}) = \frac{1}{2}\sum_i \eta_i |\nabla\varphi_i(\mathbf{r})|^2. \quad (13)$$

Electron localization function: The larger the electron localization is in a region, the more likely the electron motion is confined within it. If electrons are completely localized, then they can be distinguished from the ones outside. Bader and Stephens found that the regions that have large electron localization must have large magnitudes of Fermi hole integration.[10] However, the Fermi hole is a six-dimensional function and, thus, difficult to be studied visually. Becke and Edgecombe noted that spherically averaged like-spin conditional pair probability has direct correlation with the Fermi hole and then suggested the following ELF[9]

$$\mathrm{ELF}(\mathbf{r}) = \frac{1}{1 + (D(\mathbf{r})/D_0(\mathbf{r}))^2}, \quad (14)$$

where

$$D(\mathbf{r}) = \frac{1}{2}\sum_i^{\mathrm{occ}} |\nabla\varphi_i|^2 - \frac{1}{8}\left[\frac{|\nabla\rho_\alpha(\mathbf{r})|^2}{\rho_\alpha(\mathbf{r})} + \frac{|\nabla\rho_\beta(\mathbf{r})|^2}{\rho_\beta(\mathbf{r})}\right]$$
$$D_0(\mathbf{r}) = \frac{3}{10}(6\pi^2)^{2/3}\left[\rho_\alpha(\mathbf{r})^{5/3} + \rho_\beta(\mathbf{r})^{5/3}\right]. \quad (15)$$

φ_i denotes spin orbital. $D_0(\mathbf{r})$ is the counterpart of $D(\mathbf{r})$ for noninteraction homogenous electron gas. Note that above expression is a generalization of ELF for spin-polarized problems.[24] It reduces to its original definition[9] for closed-shell system when ρ_α ($\mathbf{r}$) is equal to ρ_β ($\mathbf{r}$). Savin et al. have reinterpreted ELF in the view of kinetic energy,[25,26] which made ELF also meaningful for Kohn–Sham DFT wavefunction.[13] They indicated that $D(\mathbf{r})$ reveals the excess kinetic energy density caused by Pauli repulsion, whereas $D_0(\mathbf{r})$ can be considered as Thomas–Fermi kinetic energy density. Because $D_0(\mathbf{r})$ is introduced into ELF as a reference, what the ELF reveals is actually a relative localization.

ELF is within the range of [0,1]. A large ELF value means that electrons are greatly localized, indicating that there will be a covalent bond, a lone pair or inner shells of an atom involved. ELF has been widely used for a wide variety of systems, such as organic and inorganic small molecules,[27] atomic crystals,[25] coordination compounds,[28] clusters,[29] and for different problems, such as the atomic shell structure,[24] classifications of chemical bonding modes,[26] and verifications of charge-shift bond.[30]

An approximate version of ELF has been put forward by Tsirelson and Stash,[31] in which the actual kinetic energy term is replaced by Kirzhnits-type second-order gradient expansion

$$\frac{1}{2}\sum_i^{\mathrm{occ}} |\nabla\varphi_i|^2 \approx D_0(\mathbf{r}) + (1/72)\,|\nabla\rho(\mathbf{r})|^2/\rho(\mathbf{r}) + (1/6)\nabla^2\rho(\mathbf{r}). \quad (16)$$

With eq. (16), ELF is completely independent of the wavefunction of system of interest and then can be used conveniently to analyze electron density from X-ray diffraction data.

Localized orbital locator: Localized orbital locator (LOL) proposed by Schmider and Becke[32] is another function for characterizing electron localization.

$$\mathrm{LOL}(\mathbf{r}) = \frac{\tau(\mathbf{r})}{1 + \tau(\mathbf{r})}. \quad (17)$$

The $\tau(\mathbf{r})$ used in Multiwfn is a generalized form, which can be written as follows:

$$\tau(\mathbf{r}) = \frac{\tau^{\mathrm{LSDA}}}{\tau^{\mathrm{exact}}} = \frac{(3/10)(6\pi^2)^{2/3}[\rho_\alpha(\mathbf{r})^{5/3} + \rho_\beta(\mathbf{r})^{5/3}]}{(1/2)\sum_i^{\mathrm{occ}} |\nabla\varphi_i(\mathbf{r})|^2}. \quad (18)$$

When only alpha or beta electrons presents, the above formula returns to the original form.[32] LOL has similar expression compared with ELF. Actually, the chemically significant regions that highlighted by LOL and ELF are generally qualitative comparable, whereas Jacobsen pointed out that LOL conveys more decisive and clearer picture than ELF.[33] Obviously, LOL can be interpreted in kinetic energy way as for ELF; however, LOL can also be interpreted in view of localized orbital. Small (large) LOL value usually appears in boundary (inner) region of localized orbitals because the gradient of orbital wavefunction is large (small) in this area. The value range of LOL is the same as ELF, namely [0,1]. Like what they did for ELF, Tsirelson and Stash[34] substituted τ^{exact} in eq. (18) with the density expansion in eq. (16) and then obtained an approximate version of LOL.

Average local ionization energy: Average local ionization energy[35] is written as follows:

$$\bar{I}(\mathbf{r}) = \frac{\sum_i \rho_i(\mathbf{r})|\varepsilon_i|}{\rho(\mathbf{r})}, \quad (19)$$

where ρ_i ($\mathbf{r}$) and ε_i are the electron density function and orbital energy of the ith molecular orbital, respectively. This function

has many uses, for example, reproducing atomic shell structure, measuring electronegativity, quantifying local polarizability and hardness, and predicting sites for electrophilic or radical attack. There are many potential uses of $\bar{I}$ (**r**) waiting for further investigation. An excellent review of $\bar{I}$ (**r**) has been given by Politzer et al.[36]

Fermi hole and Fermi correlation factor function: Fermi hole function reveals the decrease of probability of finding another like-spin electron at $\mathbf{r}_2$ owing to Pauli repulsion when a electron present at $\mathbf{r}_1$. The function for σ spin electrons is defined as follows[23]:

$$h^{\sigma\sigma}(\mathbf{r}_1,\mathbf{r}_2)=\frac{\rho_2^{\sigma\sigma}(\mathbf{r}_1,\mathbf{r}_2)}{\rho_\sigma(\mathbf{r}_1)}-\rho_\sigma(\mathbf{r}_2). \tag{20}$$

The value range is from $-\rho^\sigma$ ($\mathbf{r}_2$) to zero. For single-determinant wavefunctions, this function can be explicitly written as follows:

$$h^{\sigma\sigma}(\mathbf{r}_1,\mathbf{r}_2)= -\sum_{i\in\sigma}^{\text{occ}}\sum_{j\in\sigma}^{\text{occ}}\varphi_i(\mathbf{r}_1)\varphi_j^*(\mathbf{r}_1)\varphi_i^*(\mathbf{r}_2)\varphi_j(\mathbf{r}_2)/\sum_{k\in\sigma}^{\text{occ}}|\varphi_k(\mathbf{r}_1)|^2. \tag{21}$$

Fermi correlation factor is a function closely related to Fermi hole

$$f^{\sigma\sigma}(\mathbf{r}_1,\mathbf{r}_2)=h^{\sigma\sigma}(\mathbf{r}_1,\mathbf{r}_2)/\rho_\alpha(\mathbf{r}_2). \tag{22}$$

ESP from nuclear or atomic charges:

$$V_{\text{nu}}(\mathbf{r})=\sum_A\frac{Z_A}{|\mathbf{r}-\mathbf{R}_A|}, \tag{23}$$

where $\mathbf{R}_A$ and Z_A denote position vector and nuclear charge of atom A, respectively. When *chg* file (see Section wavefunction types and file formats) is used as input, Z will stand for the atomic charge recorded in the file, at this time eq. (23) is useful for analyzing the difference between exact ESP and the ESP reproduced by atomic charges.

Promolecular and deformation properties: Promolecular real space function distribution, or say promolecular property, reflects the state after molecule formation but before electron relaxation, whereas deformation property displays the variation during electron relaxation, and they are defined respectively as follows:

$$P^{\text{pro}}(\mathbf{r})=\sum_A P_A^{\text{free}}(\mathbf{r}-\mathbf{R}_A) \tag{24}$$

$$P^{\text{def}}(\mathbf{r})=P^{\text{mol}}(\mathbf{r})-P^{\text{pro}}(\mathbf{r}), \tag{25}$$

where P^{mol} (**r**) and P^{free} (**r**) stand for any real space function mentioned above of present system and atom in free state, respectively. If real space function is chosen as electron density, then the P^{def} (**r**) is often referred as deformation density, which is very useful in bonding nature analysis.[37,38]

The topology of electron density

CPs of electron density are the positions at which $|\nabla\rho|$ vanishes (except at infinity),[11] and they can be classified into four types: (3,−3), (3,−1), (3,+1), and (3,+3), which correspond to three, two, one, and none of eigenvalues of Hessian matrix of ρ are negative, respectively. As mentioned earlier, (3,−1) generally appears between attractive atom pairs and hence called bond CP (BCP). The value of real space functions at BCP has great significance, for example, the value of ρ and the sign of $\nabla^2\rho$ at BCP are closely related to bonding strength and bond type, respectively[11]; the potential energy density, namely $(1/4)\nabla^2\rho$ (**r**) − 2G (**r**), at BCP has been shown to be highly correlated with hydrogen bond energies[39]; Noorizadeh and Shakerzadeh found that local information entropy at BCP is a good indicator of aromaticity.[40]

The maximal gradient path linking BCP and associated two local maxima of density, that is (3,−3), is termed "bond path," which reveals atomic interaction path for all kinds of bonding. The collection of bond paths is known as molecular graph, which provides an unambiguous definition of molecular structure.

Population

The main use of population analysis is to derive atomic charge, which is almost the simplest model describing charge distribution. Atomic charges are unobservable experimentally, so strictly speaking they do not have rigorous physical basis. However, the concept of atomic charge is very useful; it helps to intuitively understand basic properties of molecules, and it also has important applications in the field of quantum chemistry, molecular modeling, and chemical informatics.

Hirshfeld population: Hirshfeld population[41] is a very popular method based on deformation density partition, and Hirshfeld charge is defined as follows:

$$q_A=-\int w_A^{\text{Hirsh}}(\mathbf{r})\rho^{\text{def}}(\mathbf{r})d\mathbf{r}, \tag{26}$$

where

$$\begin{aligned}\rho^{\text{def}}(\mathbf{r})&=\rho(\mathbf{r})-\rho^{\text{pro}}(\mathbf{r})\\ \rho^{\text{pro}}(\mathbf{r})&=\sum_A\rho_A^{\text{free}}(\mathbf{r}-\mathbf{R}_A)\\ w_A^{\text{Hirsh}}(\mathbf{r})&=\rho_A^{\text{free}}(\mathbf{r}-\mathbf{R}_A)/\rho^{\text{pro}}(\mathbf{r}).\end{aligned} \tag{27}$$

ρ^{free} (**r**) is spherically averaged electron density of atom in free state. Hirshfeld charge represents the charge variation in corresponding atomic space w^{Hirsh} during molecule formation. Hirshfeld charges are qualitative consistency with general chemical concepts and insensibility to the quality of wavefunction.[42]

Atomic dipole moment corrected Hirshfeld population: Hirshfeld charges are always too small[43] and have poor reproducibility of observable quantity. The main reason may be that atomic dipole moments are completely neglected. In atomic dipole moment corrected Hirshfeld method (ADCH),[44] Hirshfeld charges are corrected by expanding atomic dipole moments to correction charges placed at neighbor atoms. ADCH atomic charges are very reasonable in chemical sense. Molecular dipole moment is exactly reproduced, and the reproducibility

of ESP is also close to the atomic charges from fitting ESP. Compared with another correction method for Hirshfeld charges, namely Hirshfeld-I,[45] the computational cost of ADCH correction is almost zero.

Voronoi deformation density population: The only difference between Voronoi deformation density (VDD) population[46] and Hirshfeld population is the partition manner of molecular space. In VDD, the Voronoi cell-like partition is used. The results of VDD are close to Hirshfeld population in general, because the magnitude of deformation density is relatively small so that different weighting function definitions would not cause too much difference in atomic charges.

Becke population: In Ref. [47], Becke proposed a weighting function for decomposing whole-space DFT integral to multiple single-center spherical integrals. Although this weighting function is not intended for population analysis, we still make an attempt to utilize it to evaluate atomic charges. The Becke charge can be defined as below, and the details of weighting function are given in original article.[47]

$$q_A = Z_A - \int w_A^{\text{Becke}}(\mathbf{r})\rho(\mathbf{r})d\mathbf{r}. \tag{28}$$

Mulliken population: Mulliken population (MPA) is the oldest population method.[48–50] Inserting linear combination equation into orthonormality condition of spin orbital yields

$$1 = \sum_a C_{a,i}^2 + 2\sum_a \sum_{b>a} C_{a,i}C_{b,i}S_{a,b}, \tag{29}$$

where S is a overlap matrix among basis functions. The first term in eq. (29) is a "local term," denoting the net population of basis function in orbital i. The second term is a "cross term," denoting the shared electrons between basis function pairs. Mulliken defined the composition of basis function a in spin orbital i as follows:

$$\Theta_{i,a} = C_{a,i}^2 + \sum_{b\neq a} C_{a,i}C_{b,i}S_{a,b}. \tag{30}$$

It is clear that in MPA each cross term $2C_{a,i}C_{b,i}S_{a,b}$ is equally partitioned to corresponding basis functions. Mulliken atomic charge can be written as follows:

$$q_A = Z_A - \sum_i \eta_i \sum_{a\in A} \Theta_{i,a}. \tag{31}$$

MPA is deprecated for practical application because of serious shortcomings: (1) poor reproducibility of observable properties; (2) the equal partition of cross term has no strict physical meaning; (3) very high basis-set dependence, especially when diffusion function is used; and (4) occasionally meaningless result occurs (population number is negative).

Löwdin population: In Löwdin population,[51] Löwdin orthogonalization[52] is performed first to eliminate cross terms in eq. (29) and then corresponding local terms are just population number. The advantage of Löwdin population relative to MPA is that the negative population number never occurs, and reproducibility of molecular dipole moment is better.[53] However, Löwdin population does not possess stronger physical meaning than MPA, because the orthogonalization procedure itself is more or less arbitrary.

Modified MPA: Some people had proposed various partition methods for cross term to improve MPA, we collectively refer them as modified MPA (MMPA). In the method proposed by Ros and Schuit,[54] eq. (30) is replaced by

$$\Theta_{i,a} = C_{a,i}^2 / \sum_b C_{b,i}^2. \tag{32}$$

Because only square of coefficients present in the formula, this method is also called C-squared population analysis (SCPA). Evidently, this definition ensures Θ positivity.

The Θ defined by Stout and Politzer[55] is as follows:

$$\Theta_{i,a} = C_{a,i}^2 + \sum_{b\neq a} w_{a,b} 2C_{a,i}C_{b,i}S_{a,b}, \tag{33}$$

where

$$w_{a,b} = C_{a,i}^2/(C_{a,i}^2 + C_{b,i}^2). \tag{34}$$

This definition has more consideration on the unbalanced nature of the cross term.

The MMPA proposed by Bickelhaupt et al.[56] can be equivalently rewritten to the form of eq. (33), but weighting function is different

$$w_{a,b} = \frac{\sum_k \eta_k C_{a,k}^2}{\sum_i \eta_i C_{a,i}^2 + \sum_j \eta_j C_{b,j}^2}. \tag{35}$$

Orbital composition

Orbital composition analysis is helpful to understand orbital intrinsic characteristics, studying reaction sites, and identifying mode of charge transfer transition. Those Θ mentioned above can be utilized in orbital composition analysis, and the quantity $\Theta_{i,a} \times 100\%$ is just the composition of basis function a in orbital i. Hirshfeld weighting function defined in eq. (27) can also be used for decomposing orbital to atoms, and the composition of atom A in orbital i is

$$\int \varphi_i^2(\mathbf{r}) w_A^{\text{Hirsh}}(\mathbf{r}) d\mathbf{r} * 100\%. \tag{36}$$

We found that this partition has greater basis-set stability and is always more reliable than use of Θ to evaluate atom composition.

Bond order

Bond order is a useful tool for characterizing bond type and measuring bond strength, and this is an artificial index;

however, some bond order definitions can be intimately connected with the experimentally measurable quantity—bond energies—the relationship is referred as BEBO in literature.[57]

Wiberg bond order Wiberg bond order is defined in the footnote of Ref. [58]

$$B_{AB} = \sum_{a\in A}\sum_{b\in B} P_{ab}^2. \quad (37)$$

Where P is single particle density matrix. This definition is only suitable for the wavefunction represented by orthogonal basis sets. This constraint conflicts with most *ab initio* wavefunctions; hence, Multiwfn automatically performs Löwdin orthogonalization before the analysis.

Mayer two-center, multicenter bond order and valence: Mayer bond order[59] is a natural extension of Wiberg bond order for nonorthogonal basis. Mayer bond order between atom A and B is defined as

$$B_{AB} = B_{AB}^{\alpha} + B_{AB}^{\beta} = 2\sum_{a\in A}\sum_{b\in B}\left[(P^{\alpha}S)_{ab}(P^{\alpha}S)_{ba} + (P^{\beta}S)_{ab}(P^{\beta}S)_{ba}\right], \quad (38)$$

In general, Mayer bond order is in good agreement with empirical bond order; for the classical single, double, and triple bonds the value is close to 1.0, 2.0, and 3.0, respectively.

Mayer bond order had been generalized to multicenter.[60–62] For arbitrary number of centers, the bond order can be expressed as follows:

$$B_{AB\ldots Z} = \sum_{a\in A}\sum_{b\in B}\cdots\sum_{z\in Z}\left[(PS)_{ab}(PS)_{bc}\ldots(PS)_{za}\right]. \quad (39)$$

Total valence measures atomic bonding capacity, and the expression given by Mayer is as follows[59]:

$$V_A = 2\sum_{a\in A}(PS)_{aa} - \sum_{a\in A}\sum_{b\in A}(PS)_{ab}(PS)_{ba}. \quad (40)$$

Free valence is defined as follows:

$$F_A = V_A - \sum_{B\neq A} B_{AB} = \sum_{a\in A}\sum_{b\in A}(P^sS)_{ab}(P^sS)_{ba}, \quad (41)$$

where P^s is spin density matrix. This quantity displays remaining capacity of forming new bonds by sharing electron pairs.

Mulliken bond order: Mulliken bond order[48–50] is the total cross term between corresponding two atoms

$$B_{AB} = \sum_i B_{AB}^i = \sum_i \eta_i \sum_{a\in A}\sum_{b\in B} 2C_{a,i}C_{b,i}S_{a,b}. \quad (42)$$

This bond order definition is deprecated for quantifying bonding strength, for which Mayer bond order generally performs better. However, Mulliken bond order is a good qualitative indicator for bonding (positive value) and antibonding (negative value).

Density-of-states of isolated systems

Density-of-states (DOS) is an important concept in solid physics.[63] It denotes the number of states in unit energy interval. In isolated systems, the energy levels are discrete, and the concept of DOS is, thus, somewhat questionable. However, if the discrete energy levels are broadened to curves artificially, DOS graph becomes a valuable tool for visually characterizing orbital compositions.[64–66]

Total DOS (TDOS) of isolated system can be written as follows:

$$\mathrm{TDOS}(E) = \sum_i \delta(E-\varepsilon_i), \quad (43)$$

where ε stands for eigenvalue of single-particle Hamiltonian, and δ is dirac delta function. If δ is replaced by a broadening function $F(x)$, continuous TDOS yields.

Partial density-of-states (PDOS) is defined as follows:

$$\mathrm{PDOS}_A(E) = \sum_i \Xi_{i,A} F(E-\varepsilon_i), \quad (44)$$

where $\Xi_{i,A}$ is composition of fragment A in orbital i, and it can be evaluated by summing up corresponding Θ terms, which has been discussed above.

The overlap density-of-states (OPDOS) between fragment A and B is defined as follows:

$$\mathrm{OPDOS}_{AB}(E) = \sum_i \mathrm{X}_{AB}^i F(E-\varepsilon_i), \quad (45)$$

where X_{AB}^i denotes the composition of total cross term between fragment A and B in orbital i.

Program

Special features

Several special features of Multiwfn are discussed as follows:

1. Very user-friendly. Quantum chemistry softwares for academic purpose are often inconvenient to use, and users need to write complex input file with consulting lengthy manual. To tackle this problem, Multiwfn is designed as an interactive program, prompts shown in each step clearly instructs users what need to do next, Multiwfn also never print obscure messages, and hence there is no any barrier even for beginners. Besides, there are more than 20 practical examples in the manual, which would be very helpful for new users.

2. No third-part plotting softwares are required. A high-level graphical library DISLIN[67] is invoked internally and automatically by Multiwfn for visualizing results, and most of the plotting parameters are adjustable by users in an interactive interface. Thus, the procedure of wavefunction analysis is remarkably simplified, especially for studying distribution of real space function.

3. Multiwfn is a semi-GUI program, that is, the majority of operations are based on command-line mode, while graphical interfaces appear when necessary. The advantage over full-GUI

design is that Multiwfn can run in silent and batch mode easily by redirection and shell scripts.

4. High efficiency. The code of Multiwfn is substantially optimized. Most parts are parallelized by OpenMP technology. For time-consuming tasks, the efficiency of Multiwfn exceeds analogous programs significantly. Meanwhile, the memory requirement is very low.

Wavefunction types and file formats

Wavefunction type supported by Multiwfn includes restricted/unrestricted single-determinant wavefunction, restricted open-shell wavefunction, and post-HF wavefunction (in natural orbital formalism). For basis function, Cartesian or spherical harmonic Gauss functions with angular moment up to *g* are supported.

Input file format supported by Multiwfn includes:

1. PROAIM wavefunction file (*wfn*): The most popular format for exchanging wavefunction information, supported by Gaussian,[68] GAMESS-US[69]/UK,[70] Firefly,[71] and Q-Chem.[72]

2. AIM extended wavefunction files (*wfx*): A newly introduced format by Gaussian09 since B.01 revision as an extension of *wfn* format.

3. Gaussian formatted checkpoint file (*fch*): For the functions relied on basis function expansion, this file type is mandatory.

4. Plot file of NBO program: Containing various orbital informations generated by NBO program,[3] such as natural atomic orbitals and natural bond orbitals.

5. Protein data bank format (*pdb*): This file type can be used as structure input for the functions that only require atom coordinates, for example, evaluation of RDG and Sign(λ_2)*ρ under promolecular approximation.

6. Charge files (*chg*): A private format, only atom coordinates and atomic charges present, the main use of this format is for analysis of ESP reproduced by atomic charges.

Graphs plotted by Multiwfn can be outputted to graphic file in publication quality; abundant graphical formats are supported, such as Postscript (ps), Portable Document Format (pdf), TIFF, Graphics Interchange Format (gif), and Portable Network Graphics (png).

Main Functions

Calculating and plotting real space functions: All real space functions mentioned in Section "real space functions" can be calculated at a point (0D), in a line (1D), in a plane (2D), or in a spatial scope (3D). Multiwfn provides very flexible ways to define the spatial region: (1) Determining by program automatically to accommodate system size. (2) Assign a center and then extend specified lengths in each direction to generate the region. The center can be assigned by inputting coordinate or defined as middle point of two atoms; the latter manner is very convenient for study intermolecular interaction. (3) Input original point and translation vectors. The number of grid points in each dimension is controlled by users. All points are evenly distributed in the calculation region.

Once the calculation is finished, users can select to visualize the data directly. For 1D and 3D cases, curve line graph and isosurface graph can be plotted, respectively. For 2D cases, five graph types are supported: (1) color-filled map; (2) contour line map; (3) relief map; (4) shaded surface map with or without projection; and (5) gradient line map with or without contour lines. The generated grid data can also be written to Gaussian cube file, which is a standard volumetric data format recognized by the majority of molecular graphics programs.

For flexibility consideration, Multiwfn preserves a blank function. This design enables the real space functions supported by Multiwfn to be arbitrarily and easily extended by users themselves. Assuming one wants to analyze Weizsäcker kinetic energy density. What is needed to do is simply filling the code *userfunc=fgrad(x,y,z,'t')**2/8/fdens(x,y,z)* into "userfunc" routine and recompile the program.

Multiwfn is able to calculate and plot promolecular and deformation property for any supported real space function. The required wavefunctions for free-state atoms can be generated by Multiwfn automatically through invoking Gaussian program. User can also choose to use the atom wavefunctions provided by themselves or use the set of prebuilt atom wavefunctions under 6-31G* basis set. Notice that Multiwfn sphericalizes atom wavefunctions internally to avoid orientation dependency before evaluation of promolecular and deformation properties.

Multiwfn permits operation between real space function from multiple wavefunctions. This function makes the studies related to multiple molecules or one molecule in different states very easy, for example, the analysis of Fukui function[73] and interfragment density transition.

Population analysis and bond order analysis: All population methods mentioned in Section "population" are supported. For MPA, the atomic population number can be further decomposed to basis functions, shells, and orbital contribution.

Multiwfn supports bond order definitions discussed in Section "bond order." The maximum number of centers of Mayer multicenter bond order analysis is six. Orbital contribution for Mulliken bond order in each orbital is printable for analyzing orbitals that are favorable or unfavorable for specific bonding.

Orbital composition analysis: In Multiwfn, orbitals can be decomposed to basis functions, shells, and atoms composition by MPA, SCPA, Stout-Politzer, and Hirshfeld methods. Fragments can be defined expediently in an interactive interface. Composition of intrafragment and interfragment in each orbital can be analyzed in detail.

Plotting DOS and spectrum: TDOS, PDOS, and OPDOS can be plotted by Multiwfn. Plain text file (recorded energies levels), Gaussian output file, *wfn*, *wfx*, and *fch* format are acceptable as input. The broadening functions supported include Gaussian, Lorentzian, and pseudo-Voigt function. Multiwfn is able to plot IR, Raman, and UV/Vis spectrum too.

Topology analysis of electron density: Multiwfn is able to search CPs of electron density by Newton's method, and several modes are provided for setting up starting point: (1) input

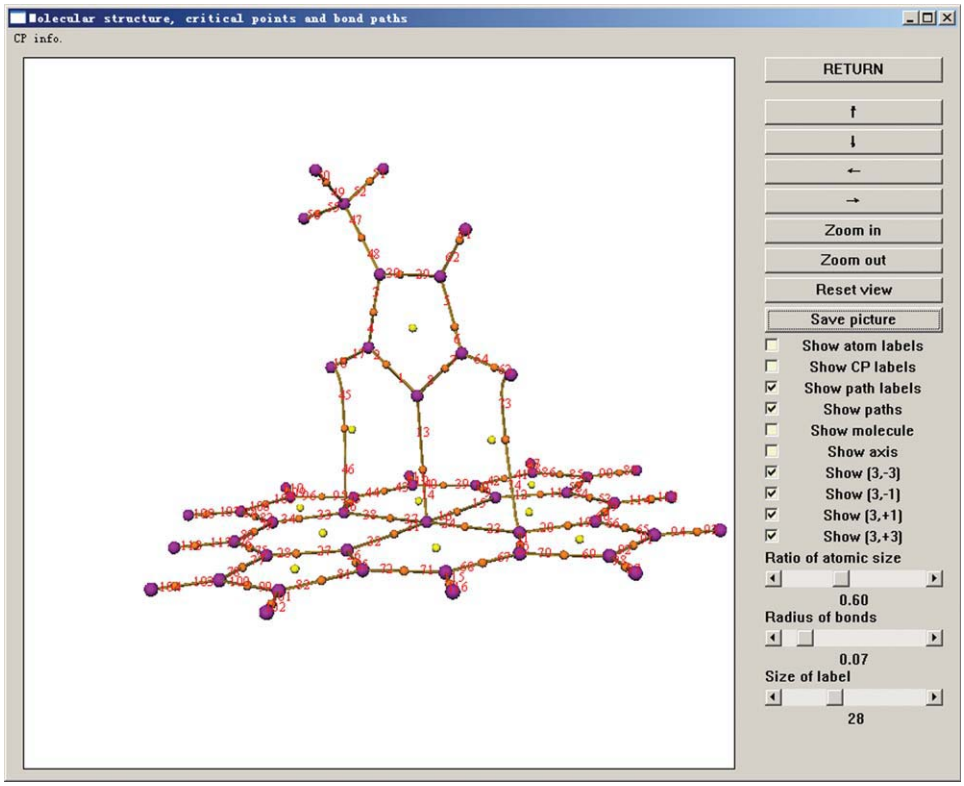

Figure 1. The interface for showing topology analysis result. Index of bond paths are labeled by red texts. Magenta, orange, and yellow spheres correspond to (3,−3), (3,−1), and (3,+1) critical points, respectively. [Color figure can be viewed in the online issue, which is available at wileyonlinelibrary.com.]

coordinate directly; (2) use nuclear positions, which are usually very close to (3,−3) type CPs; (3) use geometry center of two/three/four nuclear positions, and these modes are suitable for searching (3,−1)/(3,+1)/(3,+3) type CPs, respectively; and (4) set sphere center and radius, and then specified number of starting points are randomly distributed in the sphere. This mode is appropriate for searching the CPs that are difficult to be located by other modes.

The search of CPs is very fast, once it is finished, one can choose to generate the gradient paths that linked CPs. The results can be visualized conveniently. Figure 1 shows the CPs and gradient paths of imidazole–magnesium porphyrin complex. The value of all supported real space functions with Hessian matrix at a given CP can be printed out; CPs and paths are allowed to be added, deleted, or modified, and their detail informations can be exported out or imported in via formatted text file.

Utilities

Numerous utilities are provided in Multiwfn for facilitating wavefunction analysis and other quantum chemistry calculations. Some of them will be mentioned below.

Viewing molecular structure and orbitals: A convenient graphical interface is integrated in Multiwfn for examining molecular structure and orbitals before wavefunction analysis, see Supporting Information for screenshot.

Wavefunction examination and modification: There are plenty of options used for wavefunction examination and modification before analysis. They can be summarized into five categories: (1) Printing various informations of wavefunction in readable format. (2) Discarding or only reserving wavefunction information of specified atoms or orbitals, in which their contributions for real space functions can be eliminated or evaluated. (3) Assigning and swapping various informations of specified Gauss functions. (4) Translating and duplicating wavefunction, which is a very useful function for extending primitive cell wavefunction outputted by Gaussian to periodic wavefunction. (5) Saving modified wavefunction to new file in *wfn* format.

Analysis between two real space functions: This function enables grid data of two real space functions to be generated and outputted at the same time with sharing grid setting, and then the scatter graph between them can be drawn, which is very useful for correlation analysis. Moreover, there are options used for setting the value of one real space function, where the value of another real space function is within or without of certain range. This design particularly facilitates the visual research of weak interaction by RDG and Sign(λ_2)*ρ, and one can screen the strong interaction regions where ρ is large.

Integrating a real space function in whole space: This is a powerful function used to evaluate integral of selected real space function in whole space. By properly modifying the code of "userfunc" routine mentioned above (that is the integrand) by users, the quantity such as electric multipole moment and overlap between the norms of two orbitals can be easily obtained. The numerical method is based on the scheme proposed by Becke for integrating DFT functional.[47]

Monitoring self-consistent field convergence: The progress of self-consistent field convergence of Gaussian program can be monitored. The variations of energy, density matrix, etc. in specified step range are summarized and plotted in terms of curve map, which helps users to analyze the behavior of convergence and find solutions in ill-convergence cases.

Combining wavefunction of fragments: Multiwfn can generate Gaussian input file with initial guess that combined from multiple fragment wavefunctions. There are three primary purposes: (1) generating high-quality initial guess wavefunction for weakly interacting system. (2) Performing simple energy decomposition.

Table 2. Calculation speed of Multiwfn, DGrid, and CheckDen.

	ELF		Laplacian of ρ	
	Runtime (s)	Speed[a]	Runtime (s)	Speed[a]
CheckDen	107.3	0.10	130.2	0.10
DGrid	25.2	0.42	55.1	0.23
Multiwfn $N = 1$[b,c]	20.7	0.51	25.6	0.49
Multiwfn $N = 1$[c]	10.5	1.00	12.6	1.00
Multiwfn $N = 2$[c]	5.3	1.98	6.4	1.97
Multiwfn $N = 4$[c]	2.8	3.75	3.3	3.82

[a] The speed of Multiwfn in serial mode is considered as reference. [b] Cutoff for evaluating exponential functions is disabled, for other cases this treatment is enabled. [c] *N* denotes the number of threads in parallel implementation, similarly hereinafter.

The energy difference between the first and the last round of self-consistent field iteration can be regarded as a cause of polarization of electron density and charge transfer between fragments. (3) Studying symmetry-broken singlet state.

Efficiency

Grid data calculation is very computationally expensive. There are already some programs aiming at generating grid data for various properties, for example, DGrid[6] and CheckDen.[8] Notice that none of them supports parallel implementation. To demonstrate the high efficiency of Multiwfn, we compared their calculation speed of grid data of ELF and $\nabla^2 \rho$ for acetic acid with 6-31G** basis set[74,75] used. 88*92*77 = 623,392 points are evenly distributed in the molecular region. In consistency with public version, Multiwfn is compiled by Intel Visual Fortran Compose XE 2011 only with low-level optimization option "/O1" (for compatibility consideration); other programs are precompiled version. The CPU we used is Intel Core2 Quad Q6600.

Notice that to improve calculation speed, Multiwfn checks if the exponent is smaller than a cutoff value −40 before exactly evaluating an exponential function; if it is true, then the function will be ignored. This treatment is safe enough to ensure that loss of accuracy cannot be detected in any quantitative study of real space functions. From Table 2, it can be seen that in serial mode, Multiwfn is one order of magnitude faster than CheckDen and several times faster than DGrid. Even if the cutoff treatment is disabled, Multiwfn is still at least one time faster than DGrid for $\nabla^2 \rho$. The speedup of Multiwfn from parallel implementation is significant. When four CPU cores are available, more than 70% calculation time in serial mode could be reduced.

We also tested the performance of generating grid data for RDG and Sign(λ_2)*ρ in Multiwfn, see Supporting Information. The time consuming by Multiwfn in serial mode is comparable to or less than NCIPLOT,[76] which is a program proposed specifically for generating grid data for these two properties. Notice that NCIPLOT has not been parallelized yet.

Practical Applications

In this section, several practical examples are given to illustrate the capabilities of Multiwfn. All graphs except color-filled isosurface map are directly generated by Multiwfn; only trivial modifications have been made for clearer expression. All geometry optimizations and wavefunction calculations are performed by Gaussian03,[68] unless otherwise specified. B3LYP[77] hybrid functional is chosen as theoretical method.

ELF and Fermi hole function of CH_3Br

ecause Fermi hole of KS-DFT wavefunction is not well defined, in this example, Hartree-Fock wavefunction is used instead in combination with 6-311+G* basis set.[74,78] Figure 2 depicts ELF and Fermi hole function in the line of C—Br bond of CH_3Br molecule. The internal shells of the two atoms are clearly shown. Between carbon and bromine there is a wide and high electron localization region, which reveals that the bonding nature is covalent. As ELF is an abstract reflection of Fermi hole, it is interesting to check Fermi hole distribution when reference point is located at maximum of the bonding ELF domain. From the lower part of Figure 2, it can be seen that Fermi hole function has relatively high magnitude in the C—Br bond; meanwhile, around the two atomic nuclei there are several narrow regions with high magnitude too. Because electron can go where its hole goes,[11] the electrons shared by the two atoms are localized in the covalent bonding region to some extent, yet they are not completely confined within that region.

Molecular ESP of dihalogens

Halogen bonding is the noncovalent interaction that occurs between a halogen atom (Lewis acid) and a negative site (Lewis base).[14,79,80] It can be expressed as follows:

$$D - X \cdots B,$$

where the donor atom *D* could be an organic group or another halogen atom. It seems weird that the halogen atom *X*, which usually carries a negative charge, could act as Lewis

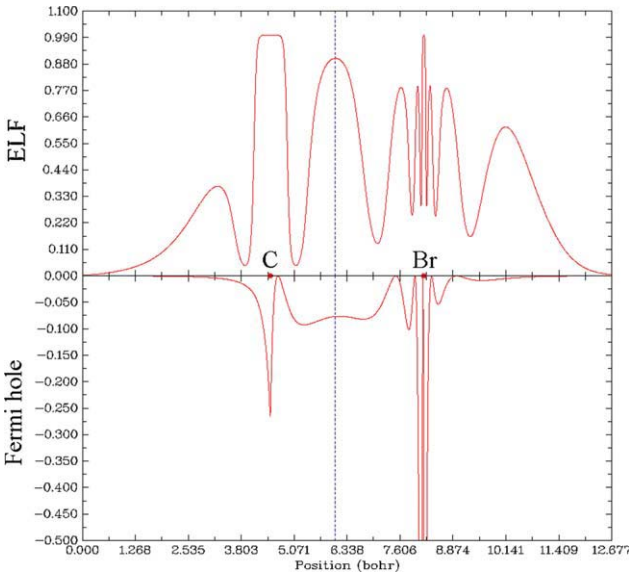

Figure 2. Electron localization function (positive part) and Fermi hole function (negative part) of CH_3Br along C—Br bond. The dashed line indicates reference position of Fermi hole function. [Color figure can be viewed in the online issue, which is available at wileyonlinelibrary.com.]

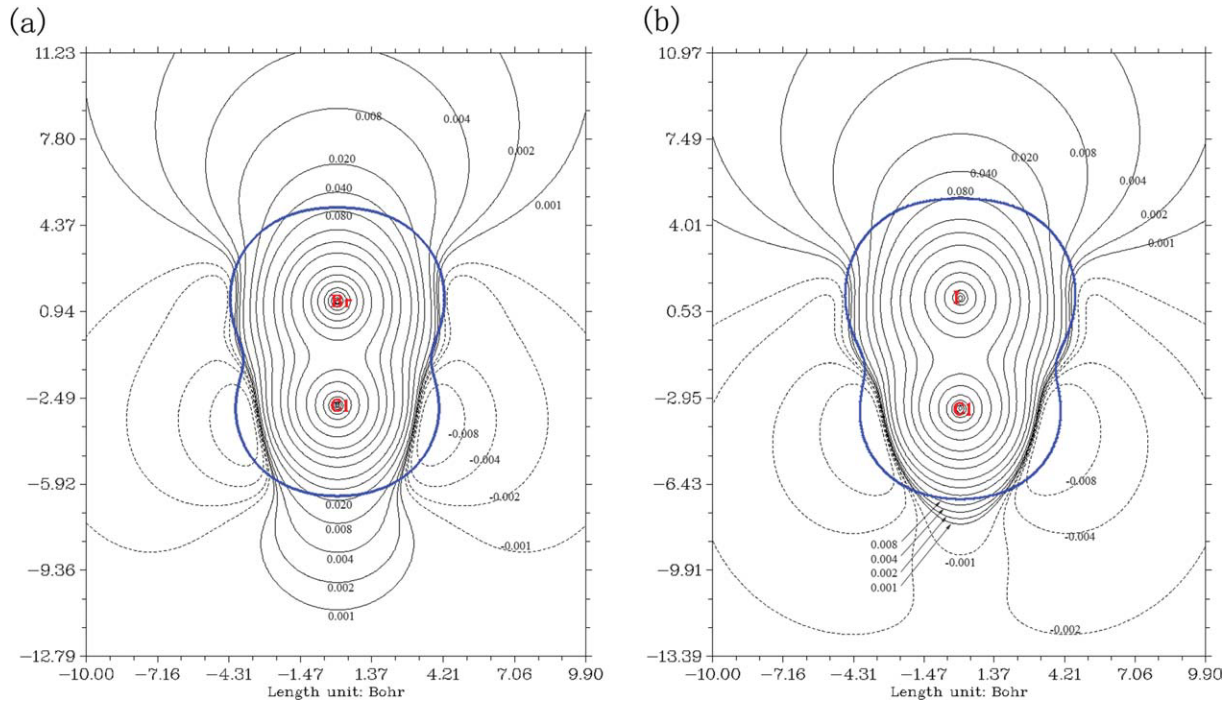

Figure 3. Contour map of ESP of (a) BrCl and (b) ICl. Blue lines denote the position where electron density equals to 0.001, which is generally regarded as molecular surface. Solid and dashed black lines are positive and negative isopotential lines, respectively. The isovalues are labeled on the graph, unit is in a.u. [Color figure can be viewed in the online issue, which is available at wileyonlinelibrary.com.]

acid. It has been found that the reason can be clearly explained by ESP. Here, we consider dihalogen molecule BrCl and ICl, in which chlorine is seen as *X*. Relativistic effective core potential Lanl[81] combining with Lanl2DZdp valence basis set[82] is utilized for iodine atom, for chlorine and bromine 6-311+G* is adopted.

The isopotential lines are shown in Figure 3, and the areas enclosed by blue lines are internal region of the molecule and will not be concerned. Because chlorine has larger electronegativity than bromine and iodine, most negative region of ESP appears in the vicinity of chlorine atom. There is an evident difference between BrCl and ICl in ESP distribution. In Figure 3a, the positive region dominated by nuclear charge of chlorine atom bulged out significantly owing to the diminution of electron density in corresponding region; meanwhile, negative region is completely separated. This is a typical nature of the halogen bonding, that is, the attractive interaction caused by electrostatic effect between the positive potential site (commonly referred as "σ-hole"[79]) of halogen atom and the electron-rich site can make system energy decreased. Because more electrons can be pulled from iodine than bromine by chlorine atom, the σ-hole in Figure 3b is largely contracted and chlorine atom is fully encompassed by dashed lines. Therefore, it can be expected that the halogen bonding is much harder to be formed in this situation.

Electron localization of B_{13}^+ and Li_6 cluster

The global minimum structure of B_{13}^+ cluster is planar with C_{2v} symmetry.[83] Figure 4 depicts its electron structure characteristic by ELF under 6-311G* basis set. It can be seen that very high value occurs between each boundary boron atom, although electrons also localized between the central atoms as well as in some regions between central and boundary atoms (e.g., B1–B11), but the extend is evidently weaker. This observation suggests that only the bonding between boundary atoms is strong. By examining Mayer bond order, this conclusion can be further verified. All two-center bond orders of adjoining atoms in boundary exceed unity, whereas bond orders between any other adjoining atoms are less than 0.6. Note that electron localization in some areas is very low, for example, between B1 and B9, and around the center of B1-B9-B10, corresponding two-center and three-center bond orders are very small (0.35 and 0.084, respectively); thus, these bonding can be expected to be very weak. Analysis of $\nabla^2 \rho$ gives similar conclusions as discussed above, see Supporting Information.

Planar D_{3h}-type structure has been found to be a local but not a global minimum on potential energy surface of Li_6 cluster.[84,85] Figure 5 shows its LOL distribution under 6-311G* basis set. It is clear that electrons are mainly localized within the three outside triangles. These regions have been known as three-center two-electron bond (3c-2e).[29] Mayer three-center bond order analysis shows that the value of outside triangle, 0.086, is much larger than the one of inner triangle, namely 0.026. It is worth noting that the red color in Figure 5 somewhat intrudes into the interstitial space between boundary atoms, and bond order of boundary Li—Li bond (0.33) is markedly larger than the inner one (0.11). Moreover, high accurate calculation[84] shows that the former bond length is slightly smaller than the latter one; hence, boundary Li—Li bonds turn out to be stronger than the inner ones.

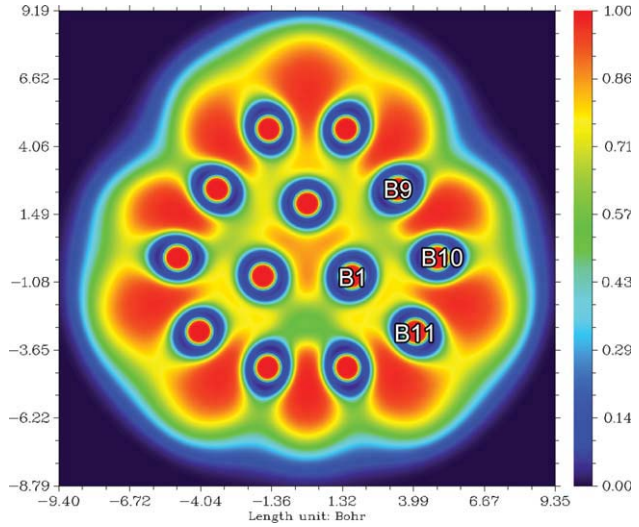

Figure 4. Color-filled map of electron localization function of planar B_{13}^+ cluster.

Weak interaction analysis of urea crystal

Here, we use RDG and Sign(λ_2)*ρ function to reveal weak interaction in urea crystal. The structure is taken from Ref. [86], and the electron density is reproduced by B3LYP/6-31G** calculation. VMD[87] is used to plot the graph. The isosurfaces in Figure 6 depict where weak interactions occur; the blue, red, and green (or earth green) colors indicate the strong attractive, strong repulsive, and van der Waals interaction, respectively. As shown by blue dashed lines, each urea molecule in crystal environment forms eight hydrogen bonds in total, oxygen atom in the urea participates in four of them. Careful inspection shows that among the four hydrogen bonds, those vertical to urea plane are slightly stronger than those parallel to the plane, because the central area of the RDG surfaces corresponding to former are more blue; actually, the length of the vertical hydrogen bonds is 0.057Å shorter than the parallel ones, whereas the electron density at the BCP corresponding to the vertical one is 15.2% larger than the parallel one. There is a small brown surface between each two adjacent ureas, as pointed out by orange arrow. This region implies the steric effect caused by close contact, which in turn is the consequence of the two hydrogen bonds around it. The surfaces crossed by magenta dashed lines, that is, the small green ellipsoids and the crooked slices, clearly exhibit the van der Waals interactions between adjacent ureas, which are easily overlooked in common interaction analysis. Another example using RDG and Sign(λ_2)*ρ function, namely the analysis of weak interaction between glycophorin A dimer, is given in Supporting Information.

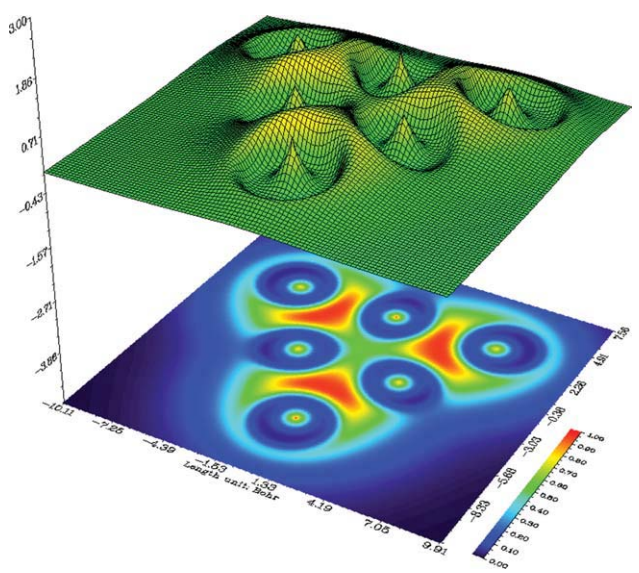

Figure 5. Relief map with projection of localized orbital locator of planar Li_6 cluster.

DOS map of ferrocene

The last example is analysis of TDOS, PDOS, and OPDOS map of ferrocene, see Figure 7. Lanl2DZ basis set combining Lanl pseudopotential is used for iron, whereas 6-31G* for other elements. Notice that only relative height rather than absolute height of curves is meaningful. *Z*-axis is perpendicular to cyclopentadienyl groups. The graph clearly exhibits orbital characteristics in different energy ranges. It is obvious that the major contribution from S, P_x and P_y basis functions of carbon (magenta curve) is due to low-lying MOs instead of frontier MOs. The major composition of MOs around −0.25 a.u. is P_z orbital of carbon (blue curve) and iron atom (red curve). Inspection of the green OPDOS curve, which expresses the bonding between carbon P_z and iron atom, suggests that carbon P_z

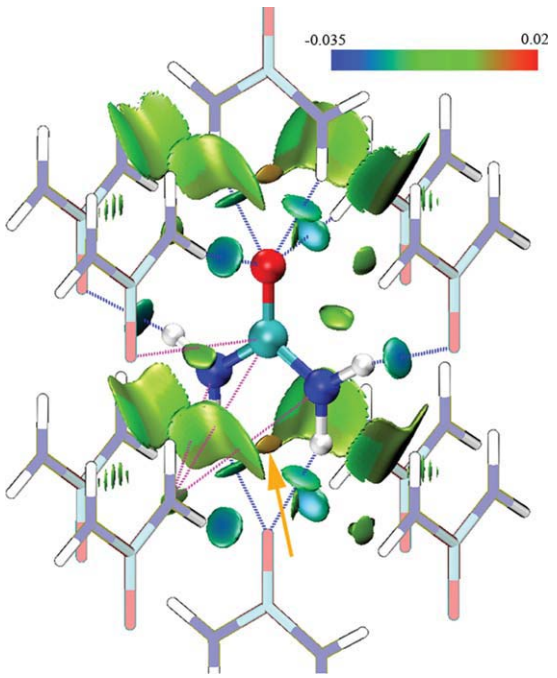

Figure 6. Reduced density gradient isosurface map with isovalue of 0.5 of urea crystal, the value of Sign(λ_2)*ρ in surfaces is represented by filling color according to the color bar in upper right corner. For clarity, the atom pairs mainly involved in hydrogen bonds and van der Waals interactions between central urea and neighbor ureas are marked by blue and magenta dashed line, respectively, orange arrow points at repulsive interaction region.

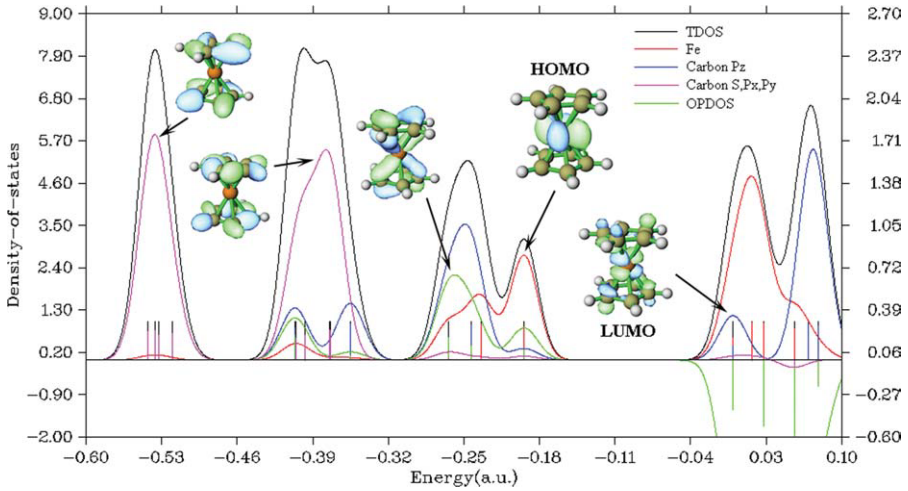

Figure 7. Total (black), partial (red, blue, and magenta), and overlap (green, between Fe and carbon P_z basis functions) density-of-states map of ferrocene. Discrete lines represent original data, the curves broadened from which have been scaled by factor of 0.05. Left axis is for total and partial density-of-states, right axis is for overlap density-of-states. Isovalue of MO isosurfaces is 0.05. The plane of cyclopentadienyl groups is perpendicular to *Z*-axis.

orbitals are very important for stabilization of ferrocene, because OPDOS has large positive value in these ranges. HOMO is almost purely contributed by iron orbitals; however, its slight overlap with carbon P_z is still beneficial to bonding. For all virtual MOs, OPDOS curve is in negative region and shows antibonding characteristic. This is due to the unfavorable overlapping in orbital phase, as can been seen from LUMO isosurface.

Conclusions

In this article, theory backgrounds, features, and functions of Multiwfn were described. The high efficiency of Multiwfn was demonstrated by comparison with related programs, and the five practical applications referring to a wide variety of systems and analysis methods were given to illustrate the capacities and usefulness of Multiwfn. Further, our program is also very easy to use for beginners.

Multiwfn will be updated continuously in the future; many new functions are already planned for succeeding versions, such as charge decomposition analysis,[64,88] plotting orbital interaction diagram, basin integral, and analysis of molecular surface properties.[7] Besides, several ELFs intended for correlation wavefunction[89–93] will be supported, and topology analysis module will be available for other real space functions soon.

Keywords: wavefunction analysis · orbital composition · population analysis · real space function · electron localization function

How to cite this article: T. Lu, F. Chen, *J. Comput. Chem.* **2012**, *33,* 580–592. DOI: 10.1002/jcc.22885

Additional Supporting Information may be found in the online version of this article.

[1] F. Jensen, Introduction to Computational Chemistry; Wiley: Chichester, **2007**; pp. 293–314.
[2] J. Cioslowski, In Encyclopedia of Computational Chemistry; P. v. R. Schleyer, Ed.; Wiley: West Sussex, **1998**; pp. 892–905.
[3] F. Weinhold, NBO, 5.0; **2001**. Available at: http://www.chem.wisc.edu/~nbo5/. Accessed on November 24, 2011.
[4] F. Biegler-König, J. Schönbohm, *J. Comput. Chem.* **2002**, *23,* 1489.
[5] S. I. Gorelsky, AOMix, 6.53; **2011**. Available at: http://www.sg-chem.net/aomix/. Accessed on November 24, 2011.
[6] M. Kohout, DGrid, 4.6; **2011**. Available at: http://www.cpfs.mpg.de/kohout/dgrid.php. Accessed on November 24, 2011.
[7] F. Bulat, A. Toro-Labbé, T. Brinck, J. Murray, P. Politzer, *J. Mol. Model.* **2010**, *16,* 1679.
[8] L. F. Pacios, A. Fernandez, *J. Mol. Graph. Model.* **2009**, *28,* 102.
[9] A. D. Becke, K. E. Edgecombe, *J. Chem. Phys.* **1990**, *92,* 5397.
[10] R. F. W. Bader, M. E. Stephens, *J. Am. Chem. Soc.* **1975**, *97,* 7391.
[11] F. W. Bader, Atoms in Molecules: A Quantum Theory; Oxford University Press: New York, **1994**.
[12] C. F. Matta, R. J. Boyd, Eds. The Quantum Theory of Atoms in Molecules—From Solid State to DNA and Drug Design; WILEY-VCH Verlag GmbH & Co. KGaA: Weinheim, **2007**.
[13] R. G. Parr, W. Yang, Density Functional Theory of Atoms and Molecules; Oxford University Press: New York, **1989**; p. 176.
[14] J. S. Murray, P. Politzer, In Encyclopedia of Computational Chemistry; P. v. R. Schleyer, Ed.; Wiley: West Sussex, **1998**; pp. 912–920.
[15] J. S. Murray, T. Brinck, P. Lane, K. Paulsen, P. Politzer, *J. Mol. Struct. (Theochem)* **1994**, *307,* 55.
[16] P. Politzer, J. S. Murray, *Theor. Chem. Acc.* **2002**, *108,* 134.
[17] C. E. Shannon, *Bell Syst Tech J* **1948**, *27,* 379.
[18] C. Aslangul, R. Constanciel, R. Daudel, P. Kottis, *Adv. Quantum. Chem.* **1972**, *6,* 93.
[19] R. G. Parr, P. W. Ayers, R. F. Nalewajski, *J. Phys. Chem. A.* **2005**, *109,* 3957.
[20] R. F. Nalewajski, R. G. Parr, *Proc. Natl. Acad. Sci. USA* **2000**, *97,* 8879.
[21] W. Koch, M. C. Holthausen, A Chemist's Guide to Density Functional Theory; Wiley-VCH Verlag GmbH: Germany, **2001**; p. 76.
[22] E. R. Johnson, S. Keinan, P. Mori-Sánchez, J. Contreras-García, A. J. Cohen, W. Yang, *J. Am. Chem. Soc.* **2010**, *132,* 6498.
[23] R. McWeeny, Methods of Molecular Quantum Mechanics; Academic Press: San Diego, **1992**; pp. 152–153.
[24] M. Kohout, A. Savin, *Int. J. Quantum. Chem.* **1996**, *60,* 875.
[25] A. Savin, O. Jepsen, J. Flad, O. K. Andersen, H. Preuss, H. G. von Schnering, *Angew. Chem. Int. Ed. Engl.* **1992**, *31,* 187.
[26] B. Silvi, A. Savin, *Nature* **1994**, *371,* 683.
[27] A. Savin, A. D. Becke, J. Flad, R. Nesper, H. Preuss, H. G. von Schnering, *Angew. Chem. Int. Ed. Engl.* **1991**, *30,* 409.
[28] M. Kohout, F. R. Wagner, Y. Grin, *Theor. Chem. Acc.* **2002**, *108,* 150.

[29] R. Rousseau, D. Marx, *Chem. Eur. J.* **2000**, *6,* 2982.
[30] S. Shaik, D. Danovich, B. Silvi, D. L. Lauvergnat, P. C. Hiberty, *Chem. Eur. J.* **2005**, *11,* 6358–6371.
[31] V. Tsirelson, A. Stash, *Chem. Phys. Lett.* **2002**, *351,* 142.
[32] H. L. Schmider, A. D. Becke, *J. Mol. Struct. (Theochem)* **2000**, *527,* 51.
[33] H. Jacobsen, *Can J Chem* **2008**, *86,* 695.
[34] V. Tsirelson, A. Stash, *Acta. Crystallogr. B.* **2002**, *58,* 780.
[35] P. Sjoberg, J. S. Murray, T. Brinck, P. Politzer, *Can. J. Chem.* **1990**, *68,* 1440.
[36] P. Politzer, J. Murray, F. Bulat, *J. Mol. Model.* **2010**, *16,* 1731.
[37] F. Wang, H. Du, J. Zhang, X. Gong, *Struct. Chem. 2011, 22, 1067.*
[38] L. Xu, J. Lv, P. Sang, J.-W. Zou, Q.-S. Yu, M.-B. Xu, *Chem. Phys.* **2011**, *379,* 66.
[39] E. Espinosa, E. Molins, C. Lecomte, *Chem. Phys. Lett.* **1998**, *285,* 170.
[40] S. Noorizadeh, E. Shakerzadeh, *Phys. Chem. Chem. Phys.* **2010**, *12,* 4742.
[41] F. L. Hirshfeld, *Theor. Chem. Acc.* **1977**, *44,* 129.
[42] B. Rousseau, A. Peeters, C. Van Alsenoy, *Chem. Phys. Lett.* **2000**, *324,* 189.
[43] E. R. Davidson, S. Chakravorty, *Theor. Chem. Acc.* **1992**, *83,* 319.
[44] T. Lu, F. Chen, *J. Theor. Comput. Chem. (in press).*
[45] P. Bultinck, C. Van Alsenoy, P. W. Ayers, R. Carbo-Dorca, *J. Chem. Phys.* **2007**, *126,* 144111.
[46] B. Rousseau, A. Peeters, C. Van Alsenoy, *J. Mol. Struct. (Theochem)* **2001**, *538,* 235.
[47] A. D. Becke, *J. Chem. Phys.* **1988**, *88,* 2547.
[48] R. S. Mulliken, *J. Chem. Phys.* **1955**, *23,* 1841.
[49] R. S. Mulliken, *J. Chem. Phys.* **1955**, *23,* 1833.
[50] R. S. Mulliken, *J. Chem. Phys.* **1955**, *23,* 2338.
[51] L. C. Cusachs, P. Politzer, *Chem. Phys. Lett.* **1968**, *1,* 529.
[52] P.-O. Löwdin, *Adv. Quantum. Chem.* **1970**, *5,* 185.
[53] J. Li, T. Zhu, C. J. Cramer, D. G. Truhlar, *J. Phys. Chem. A.* **1998**, *102,* 1820.
[54] P. Ros, G. C. A. Schuit, *Theor. Chem. Acc.* **1966**, *4,* 1.
[55] E. W. Stout, P. Politzer, *Theor. Chem. Acc.* **1968**, *12,* 379.
[56] F. M. Bickelhaupt, N. J. R. van Eikema Hommes, C. Fonseca Guerra, E. J. Baerends, *Organometallics* **1996**, *15,* 2923.
[57] H. S. Johnston, C. Parr, *J. Am. Chem. Soc.* **1963**, *85,* 2544.
[58] K. B. Wiberg, *Tetrahedron* **1968**, *24,* 1083.
[59] I. Mayer, *Chem. Phys. Lett.* **1983**, *97,* 270.
[60] A. B. Sannigrahi, T. Kar, *Chem. Phys. Lett.* **1990**, *173,* 569.
[61] T. Kar, E. Sánchez Marcos, *Chem. Phys. Lett.* **1992**, *192,* 14.
[62] R. Ponec, I. Mayer, *J Phys Chem A* **1997**, *101,* 1738.
[63] A. R. Leach, Molecular Modelling Principles and Applications; Pearson Education: Harlow, **2001**; pp. 138–164.
[64] S. I. Gorelsky, S. Ghosh, E. I. Solomon, *J. Am. Chem. Soc.* **2005**, *128,* 278.
[65] S. Ghosh, S. I. Gorelsky, P. Chen, I. Cabrito, J. J. G. Moura, I. Moura, E. I. Solomon, *J. Am. Chem. Soc.* **2003**, *125,* 15708.
[66] C. Platas-Iglesias, D. Esteban-Gómez, T. Enríquez-Pérez, F. Avecilla, A. de Blas, T. Rodríguez-Blas, *Inorg. Chem.* **2005**, *44,* 2224.
[67] Michels, H. DISLIN, 10.0; **2011**. Available at: http://www.mps.mpg.de/dislin/. Accessed on November 24, 2011.
[68] M. J. Frisch, G. W. Trucks, H. B. Schlegel, G. E. Scuseria, M. A. Robb, J. R. Cheeseman, J. A. Montgomery, Jr., T. Vrevon, K. N. Kudin, J. C. Burant, J. M. Millam, S. S. Iyengar, J. Tomasi, V. Barone, B. Menucci, M. Cossi, G. Scalmani, N. Rega, G. A. Petersson, H. Nakatsuji, M. Hada, M. Ehara, K. Toyota, R. Fukuda, J. Hasegawa, M. Ishida, T. Nakajima, Y. Honda, O. Kitao, H. Nakai, M. Klene, X. Li, J. E. Knox, H. P. Hratchian, J. B. Cross, C. Adamo, J. Jaramillo, R. Gomparts, R. E. Stratmann, O. Yazyev, A. J. Austin, R. Cammi, C. Pomelli, J. W. Ochterski, P. Y. Ayala, K. Morokuma, G. A. Voth, P. Salvador, J. J. Dannenberg, V. G. Zakrzewski, S. Dapprich, A. D. Daniels, M. C. Strain, O. Farkas, D. K. Malick, A. D. Rabuck, K. Raghavachari, J. B. Foresman, J. V. Ortiz, Q. Cui, A. G. Baboul, S. Clifford, J. Cioslowski, B. B. Stefanov, G. Liu, A. Liashenko, P. Piskorz, I. Komaromi, R. L. Martin, D. J. Fox, T. Keith, M. A. Al-Laham, C. Peng, A. Namayakkara, M. Challacombe, P. M. W. Gill, B. Johnson, W. Chen, M. Wong, C. Gonzalez, J. A. Pople. Gaussian 03, E.01; Gaussian, Inc.: Wallingford, CT, **2004**.
[69] M. W. Schmidt, K. K. Baldridge, J. A. Boatz, S. T. Elbert, M. S. Gordon, J. H. Jensen, S. Koseki, N. Matsunaga, K. A. Nguyen, S. Su, T. L. Windus, M. Dupuis, J. A. Montgomery. *J. Comput. Chem.* **1993**, *14,* 1347.
[70] M. F. Guest, I. J. Bush, H. J. J. van Dam, P. Sherwood, J. M. H. Thomas, J. H. van Lenthe, R. W. A. Havenith, J. Kendrick, *Mol. Phys.* **2005**, *103,* 719.
[71] A. A. Granovsky, Firefly, 8.0.0; **2011**. Available at: http://classic.chem.msu.su/gran/gamess/index.html. Accessed on November 24, 2011.
[72] Y. Shao, L. F. Molnar, Y. Jung, J. Kussmann, C. Ochsenfeld, S. T. Brown, A. T. B. Gilbert, L. V. Slipchenko, S. V. Levchenko, D. P. O'Neill, R. A. DiStasio Jr, R. C. Lochan, T. Wang, G. J. O. Beran, N. A. Besley, J. M. Herbert, C. Yeh Lin, T. Van Voorhis, S. Hung Chien, A. Sodt, R. P. Steele, V. A. Rassolov, P. E. Maslen, P. P. Korambath, R. D. Adamson, B. Austin, J. Baker, E. F. C. Byrd, H. Dachsel, R. J. Doerksen, A. Dreuw, B. D. Dunietz, A. D. Dutoi, T. R. Furlani, S. R. Gwaltney, A. Heyden, S. Hirata, C. Hsu, G. Kedziora, R. Z. Khalliulin, P. Klunzinger, A. M. Lee, M. S. Lee, W. Liang, I. Lotan, N. Nair, B. Peters, E. I. Proynov, P. A. Pieniazek, Y. Min Rhee, J. Ritchie, E. Rosta, C. David Sherrill, A. C. Simmonett, J. E. Subotnik, H. Lee Woodcock III, W. Zhang, A. T. Bell, A. K. Chakraborty, D. M. Chipman, F. J. Keil, A. Warshel, W. J. Hehre, H. F. Schaefer III, J. Kong, A. I. Krylov, P. M. W. Gill, M. Head-Gordon. *Phys. Chem. Chem. Phys.* **2006**, *8,* 3172.
[73] R. G. Parr, W. Yang, *J. Am. Chem. Soc.* **1984**, *106,* 4049.
[74] P. C. Hariharan, J. A. Pople, *Theor. Chem. Acc.* **1973**, *28,* 213.
[75] W. J. Hehre, R. Ditchfield, J. A. Pople, *J. Chem. Phys.* **1972**, *56,* 2257.
[76] J. Contreras-García, E. R. Johnson, S. Keinan, R. Chaudret, J.-P. Piquemal, D. N. Beratan, W. Yang, *J. Chem. Theory. Comput.* **2011**, *7,* 625.
[77] A. D. Becke, *J. Chem. Phys.* **1993**, *98,* 1372.
[78] R. Krishnan, J. S. Binkley, R. Seeger, J. A. Pople, *J. Chem. Phys.* **1980**, *72,* 650.
[79] T. Clark, M. Hennemann, J. Murray, P. Politzer, *J. Mol. Model.* **2007**, *13,* 291.
[80] P. Politzer, P. Lane, M. Concha, Y. Ma, J. Murray, *J. Mol. Model.* **2007**, *13,* 305.
[81] W. R. Wadt, P. J. Hay, *J. Chem. Phys.* **1985**, *82,* 284.
[82] C. E. Check, T. O. Faust, J. M. Bailey, B. J. Wright, T. M. Gilbert, L. S. Sunderlin, *J. Phys. Chem. A.* **2001**, *105,* 8111.
[83] A. Ricca, C. W. Bauschlicher, *Chem. Phys.* **1996**, *208,* 233.
[84] B. Temelso, C. D. Sherrill, *J. Chem. Phys.* **2005**, *122,* 064315.
[85] A. N. Alexandrova, A. I. Boldyrev, *J Chem Theory Comput* **2005**, *1,* 566.
[86] V. Zavodnik, A. Stash, V. Tsirelson, R. de Vries, D. Feil, *Acta. Crystallogr. B.* **1999**, *55,* 45.
[87] W. Humphrey, A. Dalke, K. Schulten, *J. Mol. Graph.* **1996**, *14,* 33.
[88] S. Dapprich, G. Frenking, *J. Phys. Chem.* **1995**, *99,* 9352.
[89] A. Scemama, M. Caffarel, R. Chaudret, J.-P. Piquemal, *J. Chem. Theory. Comput.* **2011**, *7,* 618.
[90] E. Matito, B. Silvi, M. Duran, M. Sola, *J. Chem. Phys.* **2006**, *125,* 024301.
[91] F. Feixas, E. Matito, M. Duran, M. Solà, B. Silvi, *J. Chem. Theory. Comput.* **2010**, *6,* 2736.
[92] M. Kohout, K. Pernal, F. R. Wagner, Y. Grin, *Theor. Chem. Acc.* **2004**, *112,* 453.
[93] M. Kohout, K. Pernal, F. R. Wagner, Y. Grin, *Theor. Chem. Acc.* **2005**, *113,* 287.

Received: 30 June 2011
Revised: 28 September 2011
Accepted: 21 October 2011
Published online on 8 December 2011